Proceedings of the 9ICEG
9th International Congress on Environmental Geotechnics
25-28 June, 2023 | Chania, Greece
© Authors: All rights reserved, 2023
https://doi.org/10.53243/ICEG2023-109

Snakeskin-Inspired Rib Patterns for Geomembranes

V. L. Gayathri[1], and P. Vangla[2]

[1]*PhD Candidate, Indian Institute of Technology Delhi, New Delhi, India, email: gayathrivenulatha@gmail.com*

[2]*Assistant Professor, Indian Institute of Technology Delhi, New Delhi, India, email: prashanth.vangla@civil.iitd.ac.in*

ABSTRACT

The interface shear response of clay soil and geomembranes with ribs inspired from the ventral scales of snakes was studied for their application as landfill liners. To this end, three different ventral scale patterns were selected and idealised to design the ribs in the study. Geomembrane prototypes with snakeskin-inspired ribs were fabricated using a Fused Filament Fabrication (FFF) 3D printer with Polylactic Acid (PLA) polymer. Geomembrane prototypes with no surface patterns and two commercial patterns were also 3D printed for comparative purposes. The interface shear response of the geomembrane prototypes with clay of low to medium plasticity obtained from a potential landfill site was investigated in an Advanced Interface Direct Shear Test Apparatus (Adv-IDS). The results of the tests show that the interface shear behaviour of the snakeskin-inspired ribs resembles that of the other commercial patterns, both of which show an increase in the shear stress values compared with the unpatterned geomembrane. The snakeskin-inspired ribs exhibit interface frictional anisotropy, and also mobilise significant inhomogeneous deformation at the interface, and show higher interface efficiency than the conventional geomembrane patterns.

Keywords: Geomembranes, Landfill Liners, Snakeskin-Inspired Ribs, Clay Soil, Inhomogeneous Deformation

1 INTRODUCTION

Soil-geomembrane interfaces are potential zones of weakness in a landfill, and understanding their interface frictional behaviour is of significant importance in determining the stability of a landfill. Poor frictional behaviour of improperly designed landfills with relatively smooth geomembranes may even lead to the failure of landfills (Bacas, Cañizal, & Konietzky, 2015; R. M. Koerner & Soong, 2000; McCartney, Zornberg, & Swan Jr., 2009; Zhao & Karim, 2018). Introducing additional roughness patterns and textures on geomembranes has been found to increase the interaction of the geomembranes with soil, thereby enhancing the frictional behaviour at the interface (Bacas, Konietzky, Berini, & Sagaseta, 2011; Hebeler, Frost, & Myers, 2005; Robert M. Koerner, 2005). The additional roughness patterns can be regular (or structured) or irregular, based on the manufacturing process and the material of the geomembrane. The choice of patterns significantly affects the shear behaviour of the interfaces, and studies have shown that structured patterns exhibit improved frictional behaviour than irregular patterns (A. Martinez & Frost, 2017).

Recently, studies have shown that the ventral scale patterns of the snakes are effective structured roughness patterns for geotechnical engineering applications. Most studies have concentrated on their ability to mobilise frictional anisotropy due to the orientation of the scale patterns (Alejandro Martinez et al., 2021; Alejandro Martinez, Palumbo, & Todd, 2019; Alejandro Martinez & O'Hara, 2021; Alejandro Martinez & Palumbo, 2018). However, Gayathri, Vangla, & Riya (2022) established that the shape of the snakeskin-inspired patterns also influences the interface shear behaviour. Thus, it is encouraging to adopt different snakeskin-inspired patterns for geotechnical engineering applications to imbibe the advantages of the efficient ventral scale patterns of the snakes.

This paper is a novel approach to introducing snakeskin-inspired ribs on geomembrane prototypes to explore their application on landfill liners. For this purpose, ventral scale patterns were selected and idealised to design the geomembrane ribs. Geomembrane prototypes with snakeskin-inspired ribs were fabricated using a Fused Filament Fabrication (FFF) 3D printer with Polylactic Acid (PLA) polymer.

Geomembrane prototypes with no patterns, a commercial ribbed pattern, and a commercial dotted pattern were also 3D printed for comparative purposes. The geomembrane prototypes were tested with a clay of low to medium plasticity obtained from a potential landfill site to investigate their interface shear behaviour. The results of the tests show that while the shear behaviour of snakeskin-inspired ribs resembles that of the commercial pattern, they exhibit high interface frictional behaviour and mobilise larger inhomogeneous plastic deformation and intra-rib clogging. The results of the experimental programme show encouraging results for adopting the snakeskin-inspired ribs for geomembranes and also add to the existing knowledge pool of bio-inspired geotechnics.

2 MATERIALS AND METHODS

2.1 Soil

The soil used in the study was obtained from a proposed landfill site in India. Figure 1 shows the grain size distribution curve, and it can be seen that the soil is essentially fine-grained with a clay + silt content of about 60%. The soil was oven-dried, pulverised, and homogenised (mixed properly) and tested as per ASTM standards to determine the properties. Table 1 gives the relevant properties of the soil and the corresponding ASTM test method, and the soil is classified as clay of low to medium plasticity (CL), as per United Soil Classification System (USCS) (ASTM D2487 – 17, 2017).

Table 1. *The properties of the clay soil*

Property	Value	Test Method
Liquid Limit (%)	37	ASTM D4318-17
Plastic Limit (%)	15.5	
Optimum Moisture Content (%)	15.6	ASTM D698-12
Maximum Dry Denisty (kN/m^3)	17.85	

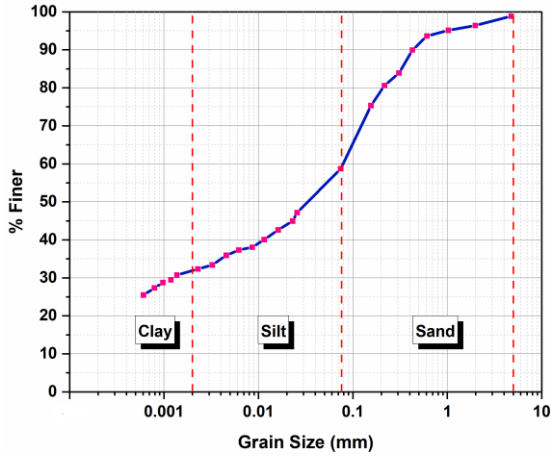

Figure 1. *Grain size distribution of the soil used in the study*

2.2 Design and fabrication of the geomembrane prototypes

The geomembrane prototypes used in the study were fabricated using 3D printing technology by employing a Fused Filament Fabrication (FFF) printer and Polylactic Acid (PLA). 3D printing technology has gained immense popularity in years as an excellent tool to develop laboratory prototypes with sophisticated and intricate patterns that were previously deemed impossible to replicate. There are numerous 3D printing technologies today; however, FFF 3D printing with PLA is one of the most widely used 3D printing methods even today across many disciplines due to the low printing temperature, easy availability, and ease of usage (Aslanzadeh, Saghlatoon, Mahdi, & Mirzavand, 2018; Jiang et al., 2016; Kumar & Krishnadas Nair, 2017; Lim et al., 2012; Sadia, So, Arafat, Isreb, & Ahmed, 2016; Singh & Singh, 2016; Tian et al., 2017). PLA is commercially available as filaments of identical properties but with different colours. Some of the relevant properties of PLA, obtained from the manufacturer, are given in Table 2. A layer thickness of 0.1 mm and an infill density of 30% were used to 3D print the geomembrane prototypes, as suggested in Gayathri & Vangla (2023). The 3D printed PLA geomembranes were found to have a Shore D hardness of 70-75D, tested as per ASTM D2240-15

(2010). The 3D printed geomembranes also have an additional secondary roughness of 28-32 μm owing to the resolution of the 3D printer, which was measured using a stylus profilometer. The 3D printed geomembranes were smoothened using sandpapers to bring down the surface roughness to 4-5 μm, which is comparable to the average surface roughness of commercial HDPE geomembranes, to remove the effect of the secondary roughness on the shear behaviour of the clay-continuum material interfaces in the study, as suggested by Gayathri & Vangla (2023).

Table 2. *Properties of PLA*[3]

Property	Value
Density, kg/m^3	1200
Softening Temperature, ^{o}C	129 -132
Melting Temperature, ^{o}C	150
Young's Modulus (MPa)	2636 ± 330
Tensile Strength (MPa)	46.6 ± 0.9

[3]Source: Raise3D Premium PLA Technical Data Sheet (2019)

The 3D printed geomembranes with outer dimensions of 180 mm (length) x 170 mm (width) consist of a patterned area of 180 mm (length) x 136 mm (width). A total of 5 geomembrane prototypes were 3D printed; 2 with snakeskin-inspired ribs, 2 with conventional geomembrane patterns that include the straight ribs and dotted patterns, and a plain one with no surface patterns (unpatterned) for comparative purposes. The snakeskin-inspired geomembrane ribs were inspired from the ventral scales of two snakes, namely, Eastern Kingsnake (EK) or *Lampropeltis getula* and Sand Boa (SB) or *Eryx conicus* that show different locomotion techniques and thrive in different habitats (adopted after Gayathri, Vangla, & Riya (2022)). The shapes of the snakeskin-inspired patterns were idealised to form the ribs with a height of 1 mm and width of 1.5 mm, spaced at a 7 mm distance. The conventional ribbed pattern (Conv_1) was also designed with a similar cross-section, while the dotted conventional geomembrane pattern (Conv_2) was designed with a height of 1 mm and a bottom width of 1.5 mm. Figure 2 presents the details of the 3D printed geomembranes used in the study. The plan view of the idealised snakeskin-inspired profiles and the conventional geomembrane patterns are shown in Figures 2 (a) and (b), respectively, and the 3D printed geomembrane prototypes are shown in Figure 2 (c). The cross-section and other details of the patterns are given in Figures 2 (d) and (e), respectively.

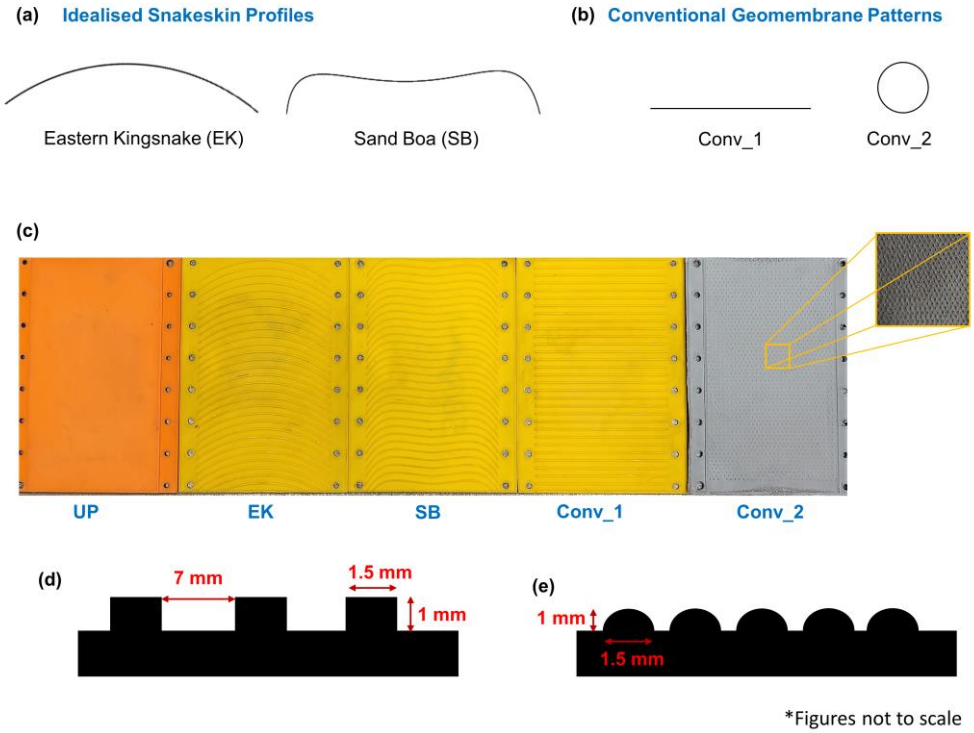

Figure 2. *Plan view of the (a) idealised snakeskin-inspired rib profiles of Eastern Kingsnake (EK) and Sand Boa (SB), and (b) conventional geomembrane patterns, (c) the 3D printed geomembrane prototypes, (d) the cross-section details of the ribs (EK, SB and Conv_1), and (e) the cross-section details of Conv_2*

The snakeskin-inspired patterns, as seen in Figure 2 (a), result in two directions of shearing. This leads to different frictional resistances in the two directions of shearing, termed frictional anisotropy. The two directions of the patterns are called cranial and caudal, pertaining to the anatomy of the snake scales, where cranial direction implies that the soil shears against the outer or convex side of the ribs and caudal direction implies that the soil shears against the inner or concave side of the ribs. Table 3 provides a description of the nomenclature used for the various continuum surfaces employed in the study.

Table 3. *Nomenclature of the different geomembrane prototypes*

Description	Direction of Shearing	Nomenclature
Eastern Kingsnake Pattern (EK)	Cranial	EK_Cr
	Caudal	EK_Cd
Sand Boa Pattern (SB)	Cranial	SB_Cr
	Caudal	SB_Cd
Conventional Ribbed Pattern	-	Conv_1
Conventional Dotted Pattern	-	Conv_2
Unpatterned (UP)	-	UP

2.3 Interface direct shear tests

An Advanced Interface Direct Shear Test Apparatus (Adv-IDS) was used for conducting the interface shear tests between the soil and the 3D printed geomembrane prototypes, as per ASTM D5321 - 08 (2008). Adv-IDS consists of a movable platform onto which continuum materials can be clamped. The clay was compacted to MDD at OMC in the shear box of inner dimensions 100 mm x 100 mm using custom-made static compaction equipment and was placed on top of the clamped continuum surface (3D printed geomembranes). The shear box was kept stationary by applying a normal load, and the platform was moved forwards at a rate of 1 mm/min using a stepper motor. A detailed description of the apparatus can be found in Gayathri et al. (2022). Each 3D printed geomembrane was tested under three normal stresses, namely, 20 kPa, 40 kPa, and 80 kPa.

3 RESULTS AND DISCUSSION

3.1 Shear response

The results of the experimental programme on the soil and 3D printed geomembrane prototypes are presented as shear stress – horizontal displacement plots and failure envelopes. The repeatability of the test results was ascertained by repeating several interface shear tests with clay and the 3D printed geomembranes. Figure 3 presents a typical repeatability result for the clay - SB_Cr interface at 20 kPa normal stress. The close match between the results of the trials is evident in Figure 3, thus confirming the repeatability of the test results. Figure 4 (a)-(c) presents the shear stress - horizontal displacement plots of all the snakeskin-inspired geomembrane prototypes and clay at 20 kPa, 40 kPa and 80 kPa normal stresses, respectively, while the shear stress - horizontal displacement plots of the conventional geomembrane patterns at 20 kPa, 40 kPa and 80 kPa normal stresses are presented in Figures 4 (d)-(f). The shear-stress horizontal displacement plots of UP are also included in Figures 4 (a)-(f) for comparative purposes. Further, it was observed that the failure envelopes of the 3D printed geomembrane prototypes and clay interfaces exhibit significant nonlinearity. Hence, non-linear failure envelopes of the form

$$\tau_p = a\sigma_n^{\,b} \tag{1}$$

where τ_p is the peak shear stress, σ_n is the applied normal stress, and a and b are constants, are fitted for all the interfaces in the study. The failure envelopes of all the interfaces in the study are given in Figure 5, and the corresponding a and b are given in Table 4.

3.1.1 Snakeskin-inspired ribbed geomembrane patterns

The snakeskin-inspired ribbed geomembranes show significantly different shear stress-horizontal displacement responses than the unpatterned geomembrane, as evident from Figures 4 (a)-(c). The peak shear stress values show a noticeable increase in the ribbed geomembranes than the unpatterned geomembrane at all three normal stresses. This difference in responses could be due to differences in

the mechanism of interaction of the clay with the different geomembranes. In the ribbed geomembranes, the ribs penetrate the soil sample, leading to substantial engagement of the soil with the ribs. During the

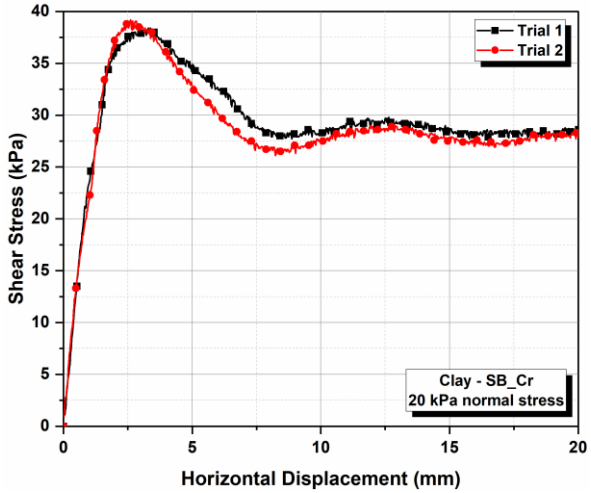

Figure 3. *Repeatability test results of SB_Cr at 20 kPa normal stress*

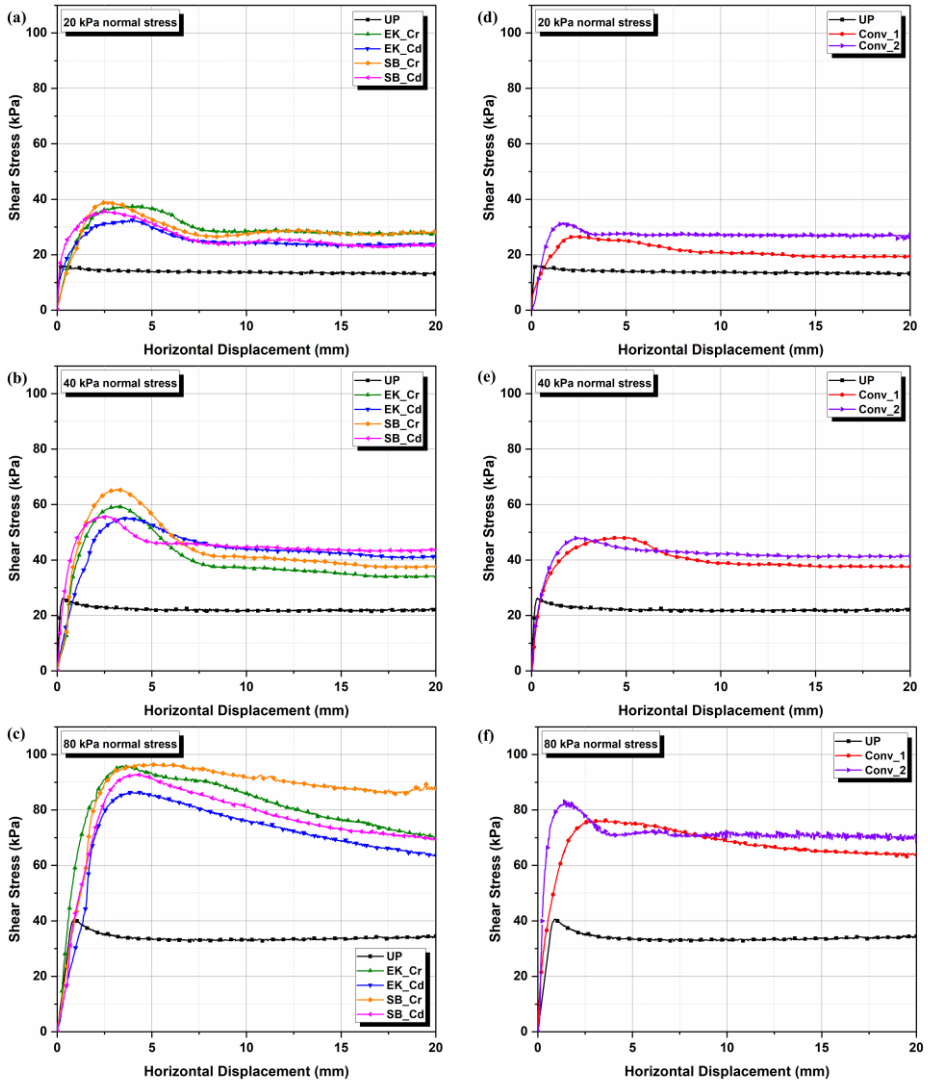

Figure 4. *The shear stress – horizontal strain behaviour of the unpatterned and snakeskin-inspired geomembrane prototypes at (a) 20 kPa, (b) 40 kPa, and (c) 80 kPa normal stress, and the conventional and unpatterned geomembrane prototypes at (d) 20 kPa, (e) 40 kPa, and (f) 80 kPa normal stress*

interface shearing, the penetrated ribs remove layers of clay soil at and around the interface, resulting in large plastic deformation and clogging at the intra-rib spaces and, consequently, larger interface shear resistances.

Table 3. *The constants a and b of the non-linear failure envelopes of the geomembrane prototypes*

Geomembrane	a	b
UP	2.14	0.67
EK_Cr	5.13	0.66
EK_Cd	3.39	0.76
SB_Cr	4.27	0.71
SB_Cd	5.37	0.65
Conv_1	2.19	0.84
Conv_2	3.80	0.7

It is also clear from Figures 4 (a)-(c) that the shape of the snakeskin-inspired ribs also affects the shear response of the clay-geomembrane interfaces. While both the snakeskin-inspired ribs show higher peak interface shear stress than the unpatterned geomembrane, the highest peak interface shear stress is mobilised by the SB pattern, followed by the EK pattern. This difference is observed at all normal stresses; however, the variation in the responses is more prominent at higher normal stresses than at 20 kPa. The higher shear stress values mobilised by the SB and EK patterns can be attributed to their more complicated geometry. Gayathri et al. (2022) introduced the Interaction Length Ratio (IL_R), which is defined as the ratio of the Length of Interaction (L_i) to the Profile Length (L_p). IL_R is the highest for the SB pattern (1.20), followed by the EK pattern (1.06). Thus, the SB pattern offers more length for the clay to interact with the ribs, leading to the highest shear resistance at the interface. The larger the IL_R, the more inhomogeneous deformation at the interface and the more is the mobilisation of the interface frictional resistance.

The peculiar feature of the snakeskin-inspired ribs is the interface frictional anisotropy due to the shape of the patterns. It is evident from Figure 4 that both EK and the SB patterns mobilise larger interface shear resistance in the cranial direction than in the caudal direction. This could be due to the convex side of the patterns in the cranial shearing leading to more inhomogeneous deformation at the interface than the concave side of the ribs in the caudal shearing in both EK and SB patterns. The convex side of EK and SB patterns have more length of interaction compared to the concave side of the patterns, which leads to more engagement of the clay with the ribs and, consequently, more shear resistance.

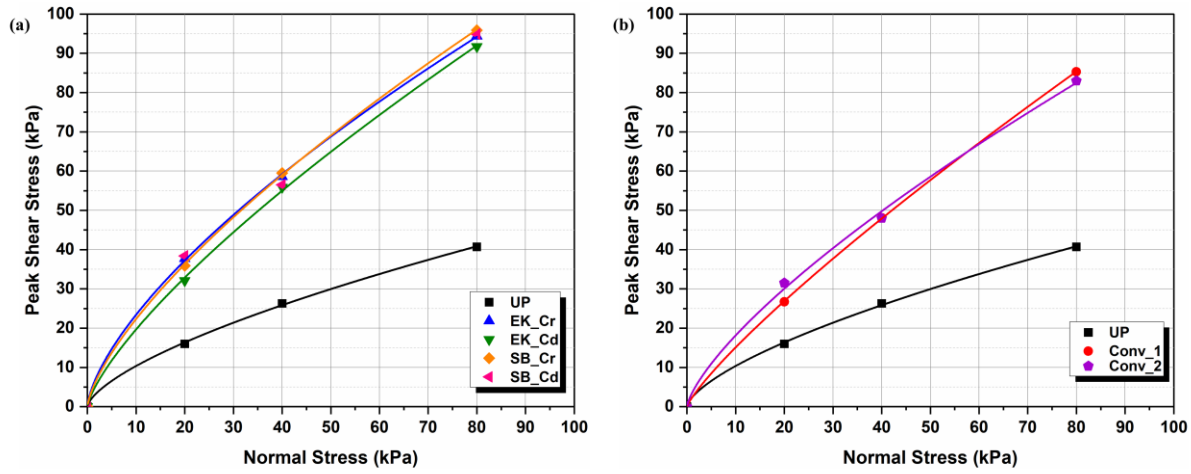

Figure 5. *Non-linear failure envelopes of (a) Snakeskin-inspired, (b) conventional geomembrane prototypes*

3.1.2 Conventional geomembrane patterns

The shear response of the conventional geomembrane patterns, as shown in Figures 4 (d)-(f), also shows an increase in the peak interface shear stress values compared to the unpatterned geomembrane. Conv_1, which is a ribbed geomembrane, and Conv_2, the dotted geomembrane prototype, show similar behaviour in both the peak and post-peak behaviour. However, there appears

to be more uniformity in the responses of Conv_2 at all the normal stresses than Conv_1. The variation could be due to differences in the interaction between the ribs and the dotted pattern of Conv_1 and Conv_2, respectively. Similar to the snakeskin-inspired ribs, ribs of Conv_1 also penetrate the clay under normal stress and leads to non-homogeneous deformation at the interface during shearing. The dotted protrusions of Conv_2, however, do not penetrate as much as the ribs, leading to comparatively more uniform deformation at the interface than Conv_1.

3.1.3 Comparison of the snakeskin-inspired and conventional geomembrane patterns

It can be seen from Figures 4 and 5 that there is a significant increase in the peak interface shear strength in both snakeskin-inspired and conventional patterns when compared to the unpatterned geomembrane. The snakeskin-inspired ribs mobilise a higher peak interface shear strength than the conventional patterns, which could be due to their intricate geometry. However, it can be seen that there are similarities in the interface shear behaviour of the snakeskin-inspired ribs and the conventional geomembrane patterns. The pre-peak, peak and post-peak behaviours of the snakeskin-inspired patterns align more with the ribbed Conv_1 than Conv_2. For instance, Table 5 presents the peak secant modulus of all the geomembrane interfaces used in the study. It is clear from the study that the ribbed geomembranes (EK, SB and Conv_1) have lower secant modulus at all normal stresses than Conv_2 and UP. This could be due to the complex phenomena of inhomogeneous plastic deformation at the interface that prolongs the mobilisation of the peak shear strength at the ribbed geomembranes than Conv_2 and UP.

Table 4. *Secant modulus of the geomembrane interfaces (kPa)*

Geomembrane	**Secant Modulus (kPa)**		
	20 kPa	**40 kPa**	**80 kPa**
UP	757	900	1100
EK_Cr	106	143	196
EK_Cd	84	144	227
SB_Cr	117	150	216
SB_Cd	95	144	267
Conv_1	92	149	191
Conv_2	192	206	235

It is also evident from Figure 4 that Conv_2 and UP show an evident peak shear stress, followed by an immediate reduction in strength post-peak that becomes constant as the horizontal strain increases. This post-peak reduction in strength, termed strain-softening, is also seen in the ribbed geomembranes. However, the strain-softening in the ribbed geomembranes is not as immediate as Conv_2 and UP but rather spread over more horizontal strain. However, unlike Conv_2 and UP, the pattern of strain-softening is different at different normal stresses in the ribbed geomembranes. The strain-softening values of the ribbed geomembranes are more at 20 kPa, followed by 40 kPa and then 80 kPa. It is interesting to notice that as normal stresses increase, the horizontal strain required to reach constant shear stress increases for the ribbed geomembranes. At 80 kPa normal stress, it can be seen that the shear strength has not reached a constant value, even 20% horizontal strain in the ribbed geomembranes. The strain-softening in the clay-geomembrane interfaces can be attributed to the progressive loss of shear strength at the interfaces due to the removal of clay with horizontal displacement. However, the difference in the strain softening exhibited by the ribbed geomembranes could be due to the difference in the interaction of the ribs with the clay, compared to UP and Conv_2.

All the geomembrane interfaces in the study show significant nonlinearity of the failure envelopes, as seen from Figure 5 and Table 4, compared to UP, which shows almost a linear trend of increase of peak shear stress with normal stress. The nonlinearity of the failure envelopes also seems more pronounced for the ribbed geomembranes than for the Conv_2 geomembrane. Thus, it is evident that the behaviour of the patterned geomembranes is significantly affected by the applied normal stress, which is further discussed in the subsequent sections.

3.2 Performance of the geomembrane prototypes: Effect of the applied normal stress

The results of the clay-snakeskin-inspired geomembrane tests indicate that the performance of the snakeskin-inspired ribs is significantly affected by the applied normal stress. The interface efficiency of the clay-geomembrane interfaces, defined as the ratio of the peak interface shear stress to the peak

shear strength of the clay at the corresponding normal stress, is used to evaluate and compare the performance of the different geomembrane interfaces in the study. The variation of the interface efficiency of the unpatterned and the snakeskin-inspired ribs at 20 kPa, 40 kPa and 80 kPa normal stresses is shown in Figure 6.

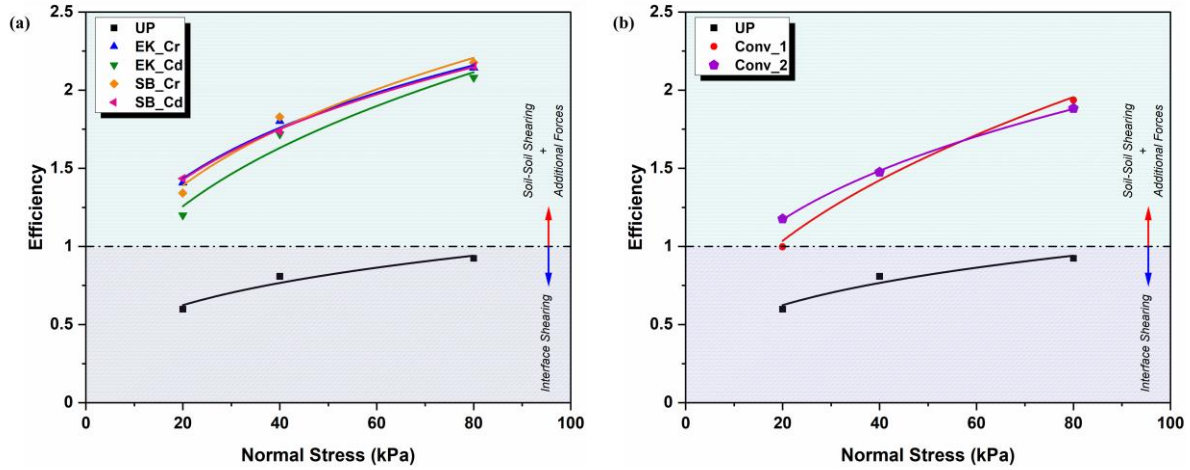

Figure 6. *Variation of interface efficiency with normal stress for (a) snakeskin-inspired geomembrane prototypes, and (b) conventional geomembrane prototypes*

Interestingly, the interface efficiency of all the clay and geomembrane interfaces shows an increase with an increase in normal stress, as evident from Figure 6. This is in contrast to sand–geomembrane interfaces found in other studies, where the interface efficiency decreases with an increase in normal stress due to the larger confinement to the displacement of the sand particles at higher normal stresses that shifts the failure plane into the soil (DeJong & Westgate, 2005; Dove & Frost, 1999; A. Martinez & Frost, 2017). The efficiency of both snakeskin-inspired and conventional geomembrane prototypes are higher than the UP at all normal stresses. The efficiency of the snakeskin-inspired patterns is higher than the conventional patterns at all normal stresses and also increases at a higher rate than the conventional patterns. This variation can be attributed to the large plastic deformation and clogging of the clay sample due to the interaction with the rib patterns. The shape of EK and SB also leads to more inhomogeneous deformations at the interface than the straight Conv_1 ribs and the Conv_2 pattern. The interaction of the ribs increases at higher normal stresses due to more penetration of the ribs into the clay and, consequently, more removal of and clogging of the intra-rib spaces, which leads to higher interface efficiency.

While the snakeskin-inspired rib patterns behave in a similar manner to the conventional geomembrane patterns, it appears that they mobilise higher plastic deformation and clogging at the interface, especially at higher normal stress, than the conventional geomembrane patterns. This behaviour is in conformance with the ventral scales of the snakes, which mostly experience low effective normal stress, typically around 10 kPa (Alejandro Martinez et al., 2019).

4 CONCLUSIONS

The paper presents a novel concept of snakeskin-inspired ribbed patterns on geomembranes for their use as liners in landfills. The following are the conclusions from the experimental study:

- The snakeskin-inspired geomembrane prototypes, like the conventional patterns, show an increase in the shear stress mobilised at the interface than an unpatterned geomembrane prototype. The interface shear response of the snakeskin-inspired geomembrane prototypes resembles that of the conventional geomembrane patterns, albeit with increased shear stress values. The SB, EK and Conv_1 patterns induce considerable intra-rib clogging and inhomogeneous plastic deformation at the interface than the Conv_2 pattern.

- The snakeskin-inspired ribs exhibit frictional anisotropy, as the shear stress in the cranial direction is found to be more than in the caudal direction. Irrespective of the direction of

shearing, the snakeskin-inspired patterns mobilise higher shear stress values than the conventional patterns. The interface shear response of the snakeskin-inspired patterns is also influenced by the shape of the patterns. The SB pattern, with a more interaction length ratio, mobilises more shear stress than the EK pattern, with a smaller interaction length ratio.

- The efficiency of snakeskin-inspired and conventional geomembrane prototypes increases with an increase in the applied normal stress. The efficiency of the snakeskin-inspired patterns is higher than the conventional patterns at all normal stress due to the difference in the interaction of the snakeskin-inspired and conventional patterns. Increased clogging and inhomogeneous plastic deformation of the clay at the interface is noticed in the ribbed geomembranes, especially at higher normal stresses.

5 ACKNOWLEDGEMENTS

The work is supported by the Science and Engineering Research Board (SERB), India (Project code: SRG/2019/000561).

REFERENCES

Aslanzadeh, S., Saghlatoon, H., Mahdi, M., & Mirzavand, R. (2018). Investigation on electrical and mechanical properties of 3D printed nylon 6 for RF / microwave electronics applications. Additive Manufacturing, 21(February), 69–75. https://doi.org/10.1016/j.addma.2018.02.016

ASTM D2240-15. (2010). Standard Test Method for Rubber Property—Durometer Hardness. ASTM International, 05(Reapproved), 1–13. https://doi.org/10.1520/D2240-15R21.2.

ASTM D2487 – 17. (2017). Standard Practice for Classification of Soils for Engineering Purposes (Unified Soil Classification System). ASTM International, 04. https://doi.org/10.1520/D2487-17.

ASTM D5321 - 08. (2008). Standard Test Method for Determining the Coefficient of Soil and Geosynthetic or Geosynthetic and Geosynthetic Friction by the Direct Shear Method. ASTM International, (Reapproved), 1–7.

Bacas, B. M., Cañizal, J., & Konietzky, H. (2015). Shear strength behavior of geotextile/geomembrane interfaces. Journal of Rock Mechanics and Geotechnical Engineering, 7(6), 638–645. https://doi.org/10.1016/j.jrmge.2015.08.001

Bacas, B. M., Konietzky, H., Berini, J. C., & Sagaseta, C. (2011). A new constitutive model for textured geomembrane/geotextile interfaces. Geotextiles and Geomembranes, 29(2), 137–148. https://doi.org/10.1016/j.geotexmem.2010.10.014

DeJong, J. T., & Westgate, Z. J. (2005). Role of overconsolidation on sand-geomembrane interface response and material damage evolution. Geotextiles and Geomembranes, 23(6), 486–512. https://doi.org/10.1016/j.geotexmem.2005.04.001

Dove, J. E., & Frost, J. D. (1999). Peak friction behavior of smooth geomembrane-particle interfaces. Journal of Geotechnical and Geoenvironmental Engineering, 125(7), 544–555. https://doi.org/10.1061/(ASCE)1090-0241(1999)125:7(544)

Gayathri, V. L., & Vangla, P. (2023). Experimental Investigation of the Suitability of 3D Printing for Soil- Continuum Interface Studies. *Geo-Congress 2023*, 497–506. Reston, VA: American Society of Civil Engineers. https://doi.org/10.1061/9780784484685.050

Gayathri, V. L., Vangla, P., & Riya, A. (2022). Effect of snakeskin-inspired patterns on the shear response of soil - continuum interfaces. International Journal of Geotechnical Engineering, 16(6), 759–775. https://doi.org/10.1080/19386362.2022.2066049

Hebeler, G. L., Frost, J. D., & Myers, A. T. (2005). Quantifying hook and loop interaction in textured geomembrane-geotextile systems. Geotextiles and Geomembranes, 23(1), 77–105. https://doi.org/10.1016/j.geotexmem.2004.06.002

Jiang, Q., Feng, X., Song, L., Gong, Y., Zheng, H., & Cui, J. (2016). Modeling rock specimens through 3D printing: Tentative experiments and prospects. Acta Mechanica Sinica/Lixue Xuebao, 32(1), 101–111. https://doi.org/10.1007/s10409-015-0524-4

Koerner, R. M., & Soong, T. Y. (2000). Leachate in landfills: The stability issues. Geotextiles and Geomembranes. https://doi.org/10.1016/S0266-1144(99)00034-5

Koerner, Robert M. (2005). *Designing with Geosynthetics* (Fifth). New Jersey: Pearson Education, Inc.

Kumar, L. J., & Krishnadas Nair, C. G. (2017). Current trends of additive manufacturing in the aerospace industry. In *Advances in 3D printing & additive manufacturing technologies* (pp. 39–54). Springer.

L., G. V, & Prashanth, V. (2023, April 7). Experimental Investigation of the Suitability of 3D Printing for Soil-Continuum Interface Studies. Geo-Congress 2023, pp. 497–506. https://doi.org/doi:10.1061/9780784484685.050

Lim, S., Buswell, R. A., Le, T. T., Austin, S. A., Gibb, A. G. F., & Thorpe, T. (2012). Developments in construction-scale additive manufacturing processes. Automation in Construction, 21, 262–268. https://doi.org/10.1016/j.autcon.2011.06.010

Martinez, A., & Frost, J. D. (2017). The influence of surface roughness form on the strength of sand – structure interfaces. Geotechnique Letters, 7(1), 104–111. https://doi.org/10.1680/jgele.16.00169

Martinez, Alejandro, Dejong, J., Akin, I., Aleali, A., Arson, C., Atkinson, J., … Zheng, J. (2021). Bio-inspired geotechnical engineering: principles, current work, opportunities and challenges. Géotechnique, 1–19. https://doi.org/10.1680/jgeot.20.p.170

Martinez, Alejandro, & O'Hara, K. (2021). Skin friction directionality in monotonically- and cyclically-loaded bio-inspired piles in sand. Deep Foundation Institute Journal, 15(1), 1–15. https://doi.org/10.37308/DFIJnl.20200831.222

Martinez, Alejandro, & Palumbo, S. (2018). Anisotropic Shear Behavior of Soil-Structure Interfaces: Bio-Inspiration from Snake Skin. *IFCEE 2018*, 94–104. Orlando, Florida: ASCE. https://doi.org/10.1061/9780784481592.010

Martinez, Alejandro, Palumbo, S., & Todd, B. D. (2019). Bioinspiration for Anisotropic Load Transfer at Soil-Structure Interfaces. Journal of Geotechnical and Geoenvironmental Engineering, 145(10), 04019074-1-04019074–14. https://doi.org/10.1061/(ASCE)GT.1943-5606.0002138

McCartney, J. S. ., Zornberg, J. G. ., & Swan Jr., R. H. (2009). Analysis of a Large Database of GCL-Geomembrane Interface Shear Strength Results. Journal of Geotechnical and Geoenvironmental Engineering, 135(2), 169–176. https://doi.org/10.1061/(ASCE)1090-0241(2009)135:2(209)

Raise3D Premium PLA Technical Data Sheet. (2019). https://doi.org/https://s2.raise3d.com/public/media/2019/07/Raise3D_Premium_PLA_TDS_V4.pdf

Sadia, M., So, A., Arafat, B., Isreb, A., & Ahmed, W. (2016). *Adaptation of pharmaceutical excipients to FDM 3D printing for the fabrication of patient-tailored immediate release tablets*. 513, 659–668.

Singh, S., & Singh, R. (2016). Fused deposition modelling based rapid patterns for investment casting applications: A review. Rapid Prototyping Journal, 22(1), 123–143. https://doi.org/10.1108/RPJ-02-2014-0017

Tian, X., Jin, J., Yuan, S., Chua, C. K., Tor, S. B., & Zhou, K. (2017). Emerging 3D-Printed Electrochemical Energy Storage Devices: A Critical Review. Advanced Energy Materials, 7(17), 1700127. https://doi.org/https://doi.org/10.1002/aenm.201700127

Zhao, L., & Karim, M. (2018). Use of Geosynthetic materials in solid waste landfill design: A review of geosynthetic related stability issues. Annals of Civil and Environmental Engineering, 2, 006–015. https://doi.org/10.29328/journal.acee.1001010